Silicon-Based Hybrid Energy Cell for Self-Powered Electrodegradation and Personal Electronics

Ya Yang,[†] Hulin Zhang,[†] Yan Liu,[†] Zong-Hong Lin,[†] Sangmin Lee,[†] Ziyin Lin,[†] Ching Ping Wong,[†] and Zhong Lin Wang[†,‡,*]

[†]School of Materials Science and Engineering, Georgia Institute of Technology, Atlanta, Georgia 30332-0245, United States and [‡]Beijing Institute of Nanoenergy and Nanosystems, Chinese Academy of Sciences, China

ABSTRACT

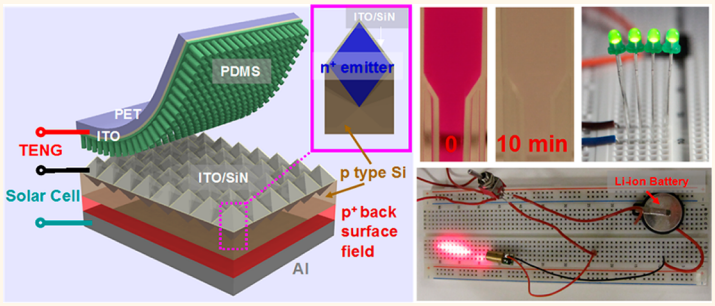

Silicon (Si)-based solar cell is by far the most established solar cell technology. The surface of a Si solar cell is usually covered by a layer of transparent material to protect the device from corrosion, contamination and mechanical damage. Here, we replaced this protection layer by a thin layer film of polydimethysiloxane nanowires. Based on this layer and using the conductive layer on the surface of the wavy Si, we have fabricated a triboelectric nanogenerator (TENG). The solar cell and the TENG form a hybrid energy cell for simultaneously harvesting solar and mechanical energies. The hybrid energy cell can be directly used for self-powered electrodegradation of rhodamine B, where the degradation percentage is up to 98% in 10 min. Moreover, the produced energy can also be stored in the Li-ion batteries for driving some personal electronics such as a red laser diode and a commercial cell phone.

KEYWORDS: hybrid energy cell · triboelectric nanogenerator · solar cells · rhodamine B · self-powered · electrodegradation

Energy harvesting from renewable and green energy resources, such as solar,[1,2] mechanical vibration,[3,4] and wasted heat,[5,6] has attracted increasing attention in the past decade due to the energy crisis and global warming. The silicon (Si)-based solar cell is so far the commercial technology for large scale harvesting of solar energy because of its low cost, superior performance, and industrial manufacturing.[7] Photon management is an effective means for improving the efficiency of a solar cell, such as fabrication of various surface pyramid structures for enhancing light absorption for increasing the solar efficiency.[8] In practical applications, the surface of a Si solar cell is usually covered by a layer of transparent material to protect the device from corrosion, contamination, and mechanical damage. When a solar cell is exposed to nature, wind becomes an existing source of energy together with the working environment of a solar cell, where wind energy can be easily converted to mechanical energy by using such flexible materials as energy harvesters. An interesting question is what if the surface layer for protecting the solar cell can be used for harvesting this kind of mechanical energy induced by wind.

Currently, nanogenerators based on the triboelectric effect have been developed to convert mechanical energy from irregular mechanical vibrations to electricity.[9,10] A triboelectric nanogenerator (TENG) can be fabricated using flexible transparent polymer materials. These materials can be a part for the TENG but can also be a surface protection layer for the solar cell, so that a hybrid energy cell technology may be fabricated to simultaneously/individually harvest multimode

* Address correspondence to zlwang@gatech.edu.

Received for review January 23, 2013 and accepted February 23, 2013.

Published online February 23, 2013
10.1021/nn400361p

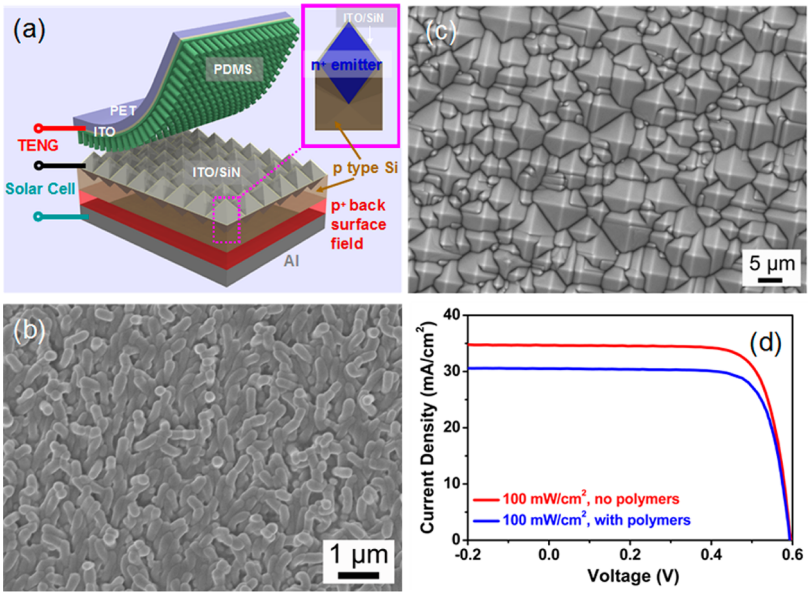

Figure 1. (a) Schematic diagram of the fabricated hybrid energy cell. (b) SEM image of the PDMS nanowire array. (c) SEM image of the fabricated Si pyramids. (d) *J*–*V* curves of the Si solar cell covered with and without PET-PDMS polymers under the light illumination intensity of 100 mW/cm^2.

energies, whichever is available. Several research efforts have been demonstrated for achieving the hybrid energy cells, but the design is not suitable for the Si-based solar cell case.[11−13] In this paper, we demonstrated a hybrid energy cell that is built directly based on a micropyramid Si solar cell for simultaneously harvesting both solar and mechanical energy. A flexible transparent polydimethysiloxane (PDMS) nanowire array-based TENG was fabricated at the top for not only harvesting the mechanical energy, but also serving as the protection layer for Si solar cell. The hybrid energy cell was used for electrodegradation of Rhodamine B (RhB) and driving some personal electronics.

RESULTS AND DISCUSSION

A schematic diagram of the fabricated hybrid energy cell is shown in Figure 1a. In this study, the PDMS nanowire array was fabricated by using a homemade anodic aluminum oxide (AAO) template, where the diameter and depth of the holes are about 200 and 500 nm, respectively. The top TENG is based on the contact/separation between the transparent PDMS nanowire array and the indium tin oxide (ITO) film. Figure 1b shows a scanning electron microscopy (SEM) image of the obtained PDMS nanowire array, revealing that the diameters are about 200 nm. The bottom Si micropyramid solar cell consists of an Al film electrode, a p^+ back surface field layer, a p type Si layer, n^+ emitter layer, SiN film, Ag grids, and the ITO film electrode.[8] The optical image of the fabricated Ag grids and the ITO film on the Si micropyramid substrate is shown in Supporting Information, Figure S1. The pyramid surface is designed to enhance the light absorption, which is also used here as an effective means for enhancing the triboelectrification process in TENG. The detailed fabrication method of the Si solar cell is given in the Experimental Section. The TENG and the Si solar cell have a coelectrode of ITO film on the Si pyramids. Figure 1c shows a SEM image of the Si pyramids, indicating that the sizes of Si pyramids are from 1 to 10 μm.

Figure 1d shows the output performance of the fabricated Si pyramid solar cell. Under the light illumination intensity of 100 mW/cm^2, the open-circuit voltage and the short-circuit current density of the device are about 0.6 V and 35 mA/cm^2, respectively. The corresponding energy conversion efficiency is up to about 16%, which is much larger than the reported Si nanowire heterojunction solar cells.[7] We also measured the output performance of the Si solar cell covered by the PDMS-PET polymers, as shown in Figure 1d. Under the same light illumination intensity, the conversion efficiency of the solar cell covered with the polymers was found to decrease from 16% to 14%.

Figure 2a shows that the output voltage of a Si solar cell device is about 0.6 V, where the corresponding output current is up to 18 mA, as shown in Supporting Information, Figure S2. By controlling the periodic contact and separation between the PDMS nanowire array and the ITO layer on the Si pyramids, the output voltage pulse of the fabricated TENG is about 3 V under the forward connection, as shown in Figure 2b. The corresponding output current and the reversed output voltage are shown in Supporting Information, Figure S3. It can be found that the TENG gives an alternating current (AC) output signal, which does not match with the direct current (DC) output signal of the Si solar cell.

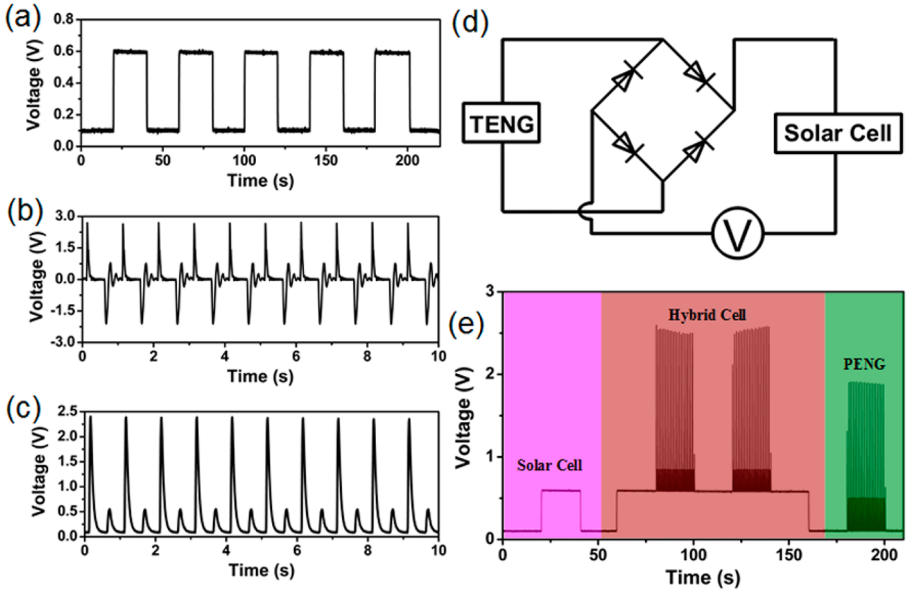

Figure 2. (a) Output voltage of the fabricated Si solar cell. (b) Output voltage of the fabricated TENG. (c) Output voltage of the TENG after the output signals were rectified. (d) Schematic diagram of the connection between the Si solar cell and TENG. (e) Output voltage of the hybrid solar cell and TENG (after rectification) for harvesting solar and mechanical energies.

A bridge rectification circuit was used to convert the AC to DC signals. The obtained rectified output voltage pulse of the device is about 2.5 V, as shown in Figure 2c. Figure 2d shows a schematic diagram of the integrated hybrid energy cell, where the solar cell and the rectified TENG device were connected in series, which can ensure that there is always a voltage/current output when either the solar or mechanical energy is available. Figure 2d shows the output voltage of the hybrid energy cell, where the output signals of TENG were rectified. It can be clearly seen that the solar cell and the TENG can work simultaneously/individually to harvest the solar and mechanical energies, respectively.

The mechanism of the TENG is to use the triboelectric effect induced electrostatic charges to drive the electrons to flow in the external circuit once the charged layers are separated by a small distance.[14] In this study, when the PDMS is in contact with the ITO film, the surface charges will be transferred from ITO to PDMS due to the electrostatic electrification, resulting in the observed output current and voltage.[15,16] The pyramid structure of the electrode largely increases the friction between the PDMS and the ITO film on the silicon surface. The output voltage V_{oc} of the TENG can be expressed by

$$V_{oc} = \frac{\sigma_0 d_S}{\varepsilon_0} - \frac{\Delta\sigma}{\varepsilon_0}\left(d_S + \frac{d_{PDMS}}{\varepsilon_{r(PDMS)}}\right) \qquad (1)$$

where σ_0 is the triboelectric charge density, $\Delta\sigma$ is the transferred charges between the two electrodes, d_S is the interlayer distance, d_{PDMS} is the thickness of the PDMS film, ε_0 is the vacuum permittivity, and $\varepsilon_{r(PDMS)}$ is the relative permittivity of PDMS.[17] According to eq 1, the output voltage V_{oc} can be increased by increasing the interlayer distance d_S. By increasing the interlayer distance and integrating five Si solar cells in series connection, Figure 3a shows that the output voltage of the hybrid cell can be increased to 12 V, which is much larger than that in Figure 2e. The corresponding output current is about 17.4 mA in Supporting Information, Figure S4.

To illustrate the potential applications of the hybrid energy cell, we demonstrated that the energy produced by the hybrid cell can be directly used for the electrodegradation of RhB and driving LEDs. RhB, as a common dyestuff found in textile wastewater, is one of the serious pollutants that are difficult to be degraded among the various dyes.[18] Electrochemical techniques possess some unique advantages in the purification of dyeing wastewater; for example, it can rapidly degrade and mineralize many organic pollutants into nontoxic small molecules by the produced hydroxyl radical OH*,[19] which is most reactive and is very strong single-electron oxidizing agent.[20] Although the electrochemical degradation of the pollutants for wastewater treatment has been extensively reported,[21,22] all of the electrochemical experiments need external power sources for the electrocatalytic oxidation. In this study, the fabricated hybrid energy cell was used to replace the external power sources to make the entire process self-powered.[23−25]

Figure 3b shows the UV−visible absorption spectra of the RhB solution for electrodegradation by using the hybrid energy cell at the same time intervals. The electrodegradation process was monitored by the characteristic absorption peak of RhB at the centered wavelength of 554 nm. It can be seen that the characteristic absorption peak intensity of RhB decreases

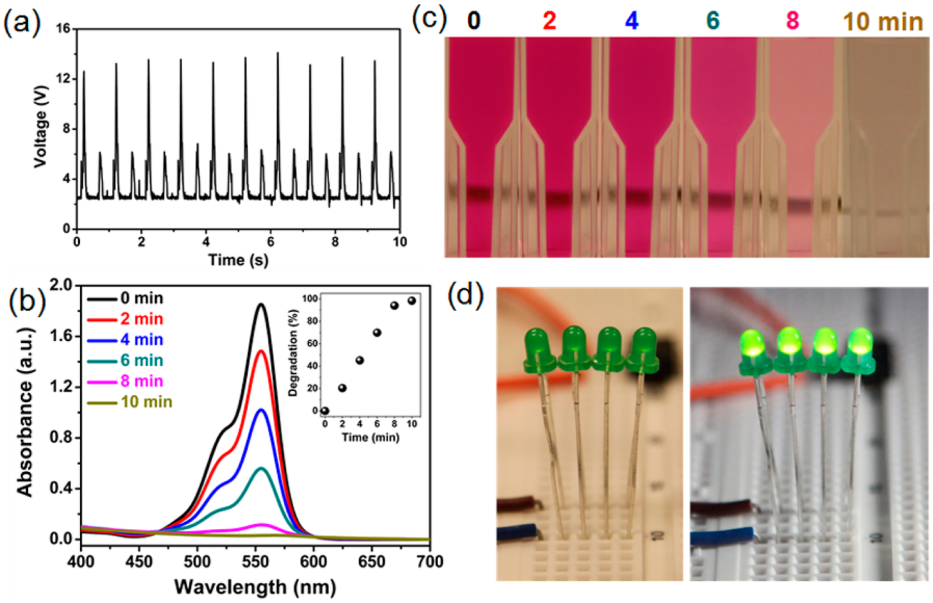

Figure 3. (a) The output voltage of the hybrid energy cell, in which five Si solar cells were integrated. (b) Absorption spectra of the RhB solution under the some time intervals. The inset shows the plot of degradation percentage versus the electrodegradation time. (c) The change in color of RhB solution under the some electrodegradation time intervals. (d) Optical images of four green LEDs before and after it was driven by the hybrid energy cell.

with increasing the electrodegradation time, indicating the decrease of the RhB concentration. The degradation percentage of RhB is up to 98% in 10 min, as shown in the inset of Figure 3b. The corresponding color change from red to colorless is shown in Figure 3c, indicating that the electrodegradation of the RhB solution can be achieved in about 10 min. To confirm that the degradation of the RhB solution is due to the energies produced by the hybrid cell, a control experiment without the connection to the hybrid energy cell was finished. There is no change in the absorption spectra of the RhB solution at the same time intervals, as shown in Supporting Information, Figure S5. In this study, NaCl was used as electrolyte in the RhB solution to improve the conductivity. The Pt electrode was used as the anode for electrocatalysis. The mechanism of the electrodegradation of RhB can be given by

$$2H_2O + Cl^- \rightarrow OH^* + ClO^- + 3H^+ + 3e^- \quad (2)$$

$$OH^*/ClO^- + RhB \rightarrow CO_2 + H_2O + NO_3^- + NH_4^+ \quad (3)$$

According to eq 2, the superoxidative hydroxyl radical OH* and ClO^- can be induced on the surface of the Pt electrode, where H_2O and Cl^- were absorbed to the anode by a discharge reaction. The RhB was then oxidized to the inorganic molecules like CO_2, H_2O, *etc.* by the superoxidative species, as shown in eq 3. Moreover, a small amount of organic molecules can be mineralized directly on the surface of the Pt electrode *via* the electrochemical combustion route.[26]

Figure 3d shows the optical images of four green LEDs before and after being driven by the fabricated hybrid cell. The observed bright green light emission indicates that these LEDs can be directly powered by the hybrid energy cell. To drive more personal electronics with the larger energy consumptions, it is necessary to store the energy produced by the hybrid cell by using some energy storage units such as Li-ion batteries. Figure 4a shows that the output voltage of the hybrid cell is about 13 V, where the corresponding output current is about 10.6 mA, as shown in Supporting Information, Figure S6. Figure 4b shows the hybrid energy cell-charging and the subsequent constant-current discharging curves of a Li-ion battery. The battery can be charged by the hybrid cell from 1.54 to 3.60 V in about 1.3 h. Under a constant discharging current of 10 mA, the discharging of the battery can last for about 580 s before it got back to the original value of 1.54 V. Thus, the stored electric capacity is up to 1.61 mAh. The charging curve in Figure 4c shows that another Li-ion battery was charged from 1.60 to 3.60 V. The inset of Figure 4c shows that the charged Li-ion battery can be used to drive a red laser diode, which is extensively used in the commercial laser pointers for the presentations. The movie file I (see the Supporting Information) also shows that the red laser diode can work under the connection with the charged Li-ion battery. Figure 4d shows that the Li-ion battery of a commercial cell phone was charged from 2.63 to 3.50 V in about 9 h, and it is ready for use (movie file II, in Supporting Information). The observed peaks in Figure 4d are associated with the Li-ion battery of the cell phone since we did not observe the similar peaks in another Li-ion battery in Figure 4b.

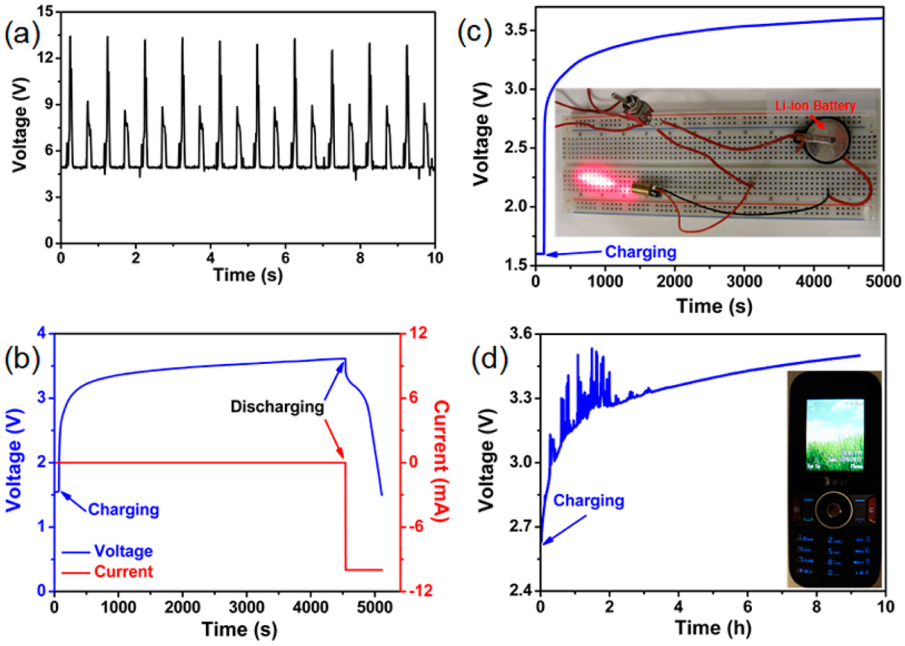

Figure 4. (a) Output voltage of the hybrid energy cell, in which 12 solar cells were integrated. (b) The hybrid energy cell-charging and the subsequent constant-current discharging curves of a Li-ion battery. (c) The charging curve of a Li-ion battery. The inset shows an optical image, where a red laser diode was driven by the charged Li-ion battery. (d) The charging curve of the Li-ion battery of a commercial cell phone. The inset shows an optical image of the cell phone driven by the Li-ion battery.

CONCLUSION

We have developed the first hybrid energy cell that consists of a solar cell and a TENG, which can be used to simultaneously/individually harvest solar and mechanical energies. The bottom solar cell device was designed by using a Si micropyramid n^+-p-p^+ junction, which can give an output voltage of 0.6 V and an output current density of 35 mA/cm^2 under the light illumination intensity of 100 mW/cm^2. The top TENG is based on the contact/separation between the PDMS nanowire array and ITO film on the Si pyramids. The output power of the hybrid energy cell can be directly used for the electrodegradation of RhB and driving LEDs. The degradation percentage of RhB is up to 98% in 10 min. The hybrid energy cell has also been used to build up a power module together with the Li-ion batteries for driving some personal electronics such as a red laser diode and a commercial cell phone. The high-power hybrid energy cells have the potential applications for self-powered electrochemical sciences (such as electrodeposition, pollutant degradation, and water splitting) and driving personal electronics (LEDs, laser diodes, and cell phones).

EXPERIMENTAL SECTION

Fabrication of the PDMS Nanowire Array and the Si Solar Cells. The AAO template was fabricated by using the industrial Al foils (99.5%). The surface energy of the AAO substrate was lowered by using a self-assembled monolayer of a heptadecafluoro-1,1,2,2-tetrahydrodecyl trichlorosilane (HDFS). PDMS was used as the nanoimprinted polymer and prepared by the gel-casting technique, which was casted on to the surface of the HDFS-coated AAO substrate. The cured PDMS nanowire array was then peeled off from the AAO substrate. The used Si substrate is a single-crystal, p-type float zone substrate with a thickness of 300 μm. The textured Si surface with pyramidal structures was created by KOH etching. The wafer was then cleaned to remove surface organic and metallic contaminants, followed by $POCl_3$ diffusion to form the n^+-emitter. A diffusion temperature of 1133 K was used for obtaining 65 Ω/sq emitter. The wafer was coated with 80 nm SiN *via* a plasma-enhanced chemical vapor deposition reactor. The SiN film serves as a passivation and antireflection coating layer for the device. After that, the screen-printed n^+-p-p^+ junction solar cells were fabricated. An Al paste was screen-printed on the backside of the Si substrate and dried at 473 K. Ag grids were then screen-printed on top of the Si substrate, followed by cofiring of both the Ag and Al contacts. During the firing step, an Al-doped Si layer, referred to as the aluminum back surface field, is also formed. An ITO top electrode with 300 nm thickness was coated by PVD 75 RF sputter. The solar cell efficiency was characterized under the light illumination intensity of 100 mW/cm^2.

Measurement of the Hybrid Energy Cell and Its Applications. In the hybrid energy cell measurement process, the bottom Si solar cell was fixed on a wooden body. The Si solar cell was covered with the PDMS nanowire array film, where one side of the film was fixed on

the wooden body by using the Kapton tape. The other side of the film was fixed on a homemade force loading system with the working frequency of 1 Hz. The fabricated TENG is based on the contact and separation between the ITO electrode on the Si solar cell and the PDMS nanowire array. Both the Si solar cell and the TENG can work under the light illumination condition. The output voltage of the device was measured by a low-noise voltage preamplifier (Keithley 6514 System Electrometer). The output current of the device was measured by a low-noise current preamplifier (Stanford Research SR560). The performance of the Li-ion battery was measured by a battery analyzer (MTI Corporation). A 3 mL aliquot of aqueous solution with the concentration of 40 mg/L RhB filling in a cuvette was prepared to carry out the RhB degradation experiment. Then, 0.1 g of NaCl as electrolyte was added into the cuvette. A Pt electrode with excellent electrochemical property was used as the anode for the electro-oxidation of RhB. At the same time intervals, an UV−visible spectrophotometer (JASCO V-630) was employed to record the absorbance spectra of the RhB solution to determine the concentration change of solution.

Conflict of Interest: The authors declare no competing financial interest.

Acknowledgment. This work was supported by Airforce, MURI, U.S. Department of Energy, Office of Basic Energy Sciences (DE-FG02-07ER46394), NSF, and the Knowledge Innovation Program of the Chinese Academy of Sciences (KJCX2-YW-M13). The authors would like to thank Ian Cooper for help with solar cell characterization.

Supporting Information Available: The additional figures about the optical image of the fabricated Ag grids and the ITO film on the Si micropyramid substrate, the output current of one solar cell device, the measured output current and voltage of the TENG under the forward and reversed connections to the measurement system in Figure 2, the output current of the hybrid energy cell in Figure 3a, the absorption spectra of the RhB solution at the same time intervals without the hybrid energy cell, and the output current of the hybrid energy cell in Figure 4a. The additional movie files include the red laser diode driven by the charged Li-ion battery and the commercial cell phone driven by the charged battery by using the hybrid cell. This material is available free of charge *via* the Internet at http://pubs.acs.org.

REFERENCES AND NOTES

1. Tian, B.; Zheng, X.; Kempa, T. J.; Fang, Y.; Yu, N.; Yu, G.; Huang, J.; Lieber, C. M. Coaxial Silicon Nanowires as Solar Cells and Nanoelectronic Power Sources. *Nature* **2007**, *6*, 885–890.
2. Jeong, S.; Garnett, E. C.; Wang, S.; Yu, Z.; Fan, S.; Brongersma, M. L.; McGehee, M. D.; Cui, Y. Hybrid Silicon Nanocone−Polymer Solar Cells. *Nano Lett.* **2012**, *12*, 2971–2976.
3. Chang, C.; Tran, V. H.; Wang, J.; Fuh, Y.-K.; Lin, L. Direct-Write Piezoelectric Polymeric Nanogenerator with High Energy Conversion Efficiency. *Nano Lett.* **2010**, *10*, 726–731.
4. Chen, X.; Xu, S.; Yao, N.; Shi, Y. 1.6 V Nanogenerator for Mechanical Energy Harvesting Using PZT Nanofibers. *Nano Lett.* **2010**, *10*, 2133–2137.
5. Liu, W.; Yan, X.; Chen, G.; Ren, Z. Recent Advances in Thermoelectric Nanocomposites. *Nano Energy* **2012**, *1*, 42–56.
6. Yang, Y.; Guo, W.; Pradel, K. C.; Zhu, G.; Zhou, Y.; Zhang, Y.; Hu, Y.; Lin, L.; Wang, Z. L. Pyroelectric Nanogenerators for Harvesting Thermoelectric Energy. *Nano Lett.* **2012**, *12*, 2833–2838.
7. Pan, C.; Luo, Z.; Xu, C.; Luo, J.; Liang, R.; Zhu, G.; Wu, W.; Guo, W.; Yan, X.; Xu, J.; *et al.* Wafer-Scale High-Throughput Ordered Arrays of Si and Coaxial $Si/Si_{1-x}Ge_x$ Wires: Fabrication, Characterization, and Photovoltaic Application. *ACS Nano* **2011**, *5*, 6629–6636.
8. Liu, Y.; Das, A.; Xu, S.; Lin, Z.; Xu, C.; Wang, Z. L.; Rohatgi, A.; Wong, C. P. Hybridizing ZnO Nanowires with Micropyramid Silicon Wafers as Superhydrophobic High-Efficiency Solar Cells. *Adv. Energy Mater.* **2012**, *2*, 47–51.
9. Fan, F.-R.; Tian, Z.-Q.; Wang, Z. L. Flexible Triboelectric Generator. *Nano Energy* **2012**, *1*, 328–334.
10. Guang, Z.; Pan, C.; Guo, W.; Chen, C.-Y.; Zhou, Y.; Yu, R.; Wang, Z. L. Tiboelectric-Generator-Driven Pulse Electrodeposition for Micropatterning. *Nano Lett.* **2012**, *12*, 4960–4965.
11. Hansen, B. J.; Liu, Y.; Yang, R.; Wang, Z. L. Hybrid Nanogenerator for Concurrently Harvesting Biomechanical and Biochemical Energy. *ACS Nano* **2010**, *4*, 3647–3652.
12. Xu, C.; Wang, Z. L. Compacted Hybrid Cell Made by Nanowire Convoluted Structured for Harvesting Solar and Mechanical Energies. *Adv. Mater.* **2011**, *23*, 873–877.
13. Pan, C.; Li, Z.; Guo, W.; Zhu, J.; Wang, Z. L. Fiber-Based Hybrid Nanogenerators for/as Self-Powered Systems in Biological Liquid. *Angew. Chem., Int. Ed.* **2011**, *50*, 11192–11196.
14. Hu, Y.; Zhang, Y.; Xu, C.; Lin, L.; Snyder, R. L.; Wang, Z. L. Self-Powered System with Wireless Data Transmission. *Nano Lett.* **2011**, *11*, 2572–2577.
15. Yang, Y.; Lin, L.; Zhang, Y.; Jing, Q.; Hou, T.-C.; Wang, Z. L. Self-Powered Magnetic Sensor Based on a Triboelectric Nanogenerator. *ACS Nano* **2012**, *6*, 10378–10383.
16. Nemeth, E.; Albrecht, V.; Schubert, G.; Simon, F. Polymer Triboelectric Charging: Dependence on Thermodynamic Surface Properties and Relative Humidity. *J. Electrostat.* **2003**, *58*, 3–16.
17. Cross, J. A. *Electrostatics: Principles, Problems and Applications*; Adam Hilger: Bristol, 1987; Chapter 2.
18. Zhou, X.; Yang, H.; Wang, C.; Mao, X.; Wang, Y.; Yang, Y.; Liu, G. Visible Light Induced Photocatalytic Degradation of Rhodamine B on One-Dimensional Iron Oxide Particles. *J. Phys. Chem. C* **2010**, *114*, 17051–17061.
19. Hua, Y.; Wang, C.; Liu, J.; Wang, B.; Liu, X.; Wu, C.; Liu, X. Visible Photocatalytic Degradation of Rhodamine B Using Fe(III)-Substituted Phosphotungstic Heteropolyanion. *J. Mol. Catal. A: Chem.* **2012**, *365*, 8–14.
20. Oturan, M. A.; Pinson, J. Hydroxylation by Electrochemically Generated OH* Radicals. Mono- and Polyhydroxylation of Benzoic Acid: Products and Isomer Distribution. *J. Phys. Chem.* **1995**, *99*, 13948–13954.
21. Mohan, N.; Balasubramanian, N.; Basha, C. A. Electrochemical Oxidation of Textile Wastewater and Its Reuse. *J. Hazard. Mater.* **2007**, *147*, 644–651.
22. Vecitis, C. D.; Gao, G.; Liu, H. Electrochemical Carbon Nanotube Filter for Adsorption, Desorption, and Oxidation of Aqueous Dyes and Anions. *J. Phys. Chem. C* **2011**, *115*, 3621–3629.
23. Xu, S.; Qin, Y.; Xu, C.; Wei, Y.; Yang, R.; Wang, Z. L. Self-Powered Nanowire Devices. *Nat. Nanotechnol.* **2010**, *5*, 366–373.
24. Wang, Z. L. Toward Self-Powered Sensor Networks. *Nano Today* **2010**, *5*, 512–514.
25. Wang, S.; Lin, L.; Wang, Z. L. Nanoscale Triboelectric-Effect-Enabled Energy Conversion for Sustainably Powering Portable Electronics. *Nano Lett.* **2012**, *12*, 6339–6346.
26. Panizza, M.; Cerisola, G. Electrocatalytic Materials for the Electrochemical Oxidation of Synthetic Dyes. *Appl. Catal. B: Environ.* **2007**, *75*, 95–101.